
Research Article: New Research | Disorders of the Nervous System

Network properties revealed during multi-scale calcium imaging of seizure activity in zebrafish

Jing Liu¹ and Scott C. Baraban¹

¹*Department of Neurological Surgery and Weill Institute for Neuroscience, University of California, San Francisco, San Francisco, CA, USA*

<https://doi.org/10.1523/ENEURO.0041-19.2019>

Received: 5 February 2019

Accepted: 8 February 2019

Published: 25 February 2019

Author contributions: J.L. and S.C.B. designed research; J.L. and S.C.B. performed research; J.L. analyzed data; J.L. and S.C.B. wrote the paper.

Funding: <http://doi.org/10.13039/100000065HHS> | NIH | National Institute of Neurological Disorders and Stroke (NINDS)
R01-NS096976
R01-NS103139

S.C.B. is a co-Founder and Scientific Advisor for EpyGenix Therapeutics.

Corresponding author: Scott C. Baraban at scott.baraban@ucsf.edu.

Cite as: eNeuro 2019; 10.1523/ENEURO.0041-19.2019

Alerts: Sign up at www.eneuro.org/alerts to receive customized email alerts when the fully formatted version of this article is published.

Accepted manuscripts are peer-reviewed but have not been through the copyediting, formatting, or proofreading process.

Copyright © 2019 Liu and Baraban

This is an open-access article distributed under the terms of the Creative Commons Attribution 4.0 International license, which permits unrestricted use, distribution and reproduction in any medium provided that the original work is properly attributed.

1 **Title:** Network properties revealed during multi-scale calcium imaging of seizure activity in zebrafish

2 **Abbreviated title:** Network properties revealed in epileptic zebrafish

3 **Authors:** Jing Liu and Scott C. Baraban

4 **Affiliation:** Department of Neurological Surgery and Weill Institute for Neuroscience, University of
5 California, San Francisco, San Francisco, CA

6 **Corresponding Author:** Scott C. Baraban, scott.baraban@ucsf.edu

7 E840 Health Sciences East, 513 Parnassus Ave., San Francisco, CA 94143

8 Number of pages: 26

9 Number of figures: 5

10 Number of movies: 6

11 Number of words: 172 (Abstract), 655(Introduction), and 920 (Discussion)

12 Acknowledgements: We would like to thank Ehud Isacoff and members of the Isacoff laboratory (Claire
13 Oldfield and Carlos Pantoja) at UC Berkeley for early training and guidance using 3i imaging calcium
14 imaging strategies in larval zebrafish. This work was supported by NIH/NINDS grants R01-NS096976,
15 R01-NS103139 and UCSF-UCB Sackler Family Exchange sabbatical fellowship (to S.C.B.).

16 Conflict of Interest: S.C.B. is a co-Founder and Scientific Advisor for EpyGenix Therapeutics.

17

18 Abstract

19 Seizures are characterized by hypersynchronization of neuronal networks. Understanding these networks
20 could provide a critical window for therapeutic control of recurrent seizure activity i.e., epilepsy. However,
21 imaging seizure networks has largely been limited to microcircuits *in vitro* or small “windows” *in vivo*.
22 Here we combine fast confocal imaging of GCaMP-expressing larval zebrafish with local field potential
23 (LFP) recordings to study epileptiform events at whole-brain and single-neuron levels *in vivo*. Using an
24 acute seizure model (pentylenetetrazole, PTZ), we reliably observed recurrent electrographic ictal-like
25 events associated with generalized activation of all major brain regions and uncovered a well-preserved
26 anterior-to-posterior seizure propagation pattern. We also examined brain-wide network synchronization
27 and spatiotemporal patterns of neuronal activity in the optic tectum microcircuit. Brain-wide and single-
28 neuronal level analysis of PTZ- and 4-aminopyridine (4-AP)-exposed zebrafish revealed distinct network
29 dynamics associated with seizure and non-seizure hyperexcitable states, respectively. Neuronal
30 ensembles, comprised of coactive neurons, were also uncovered during interictal-like periods. Taken
31 together, these results demonstrate that macro- and micro-network calcium motifs in zebrafish may
32 provide a greater understanding of epilepsy.

33

34 Significance Statement

35 Monitoring the dynamic activities in large-scale neuronal networks is critical to understanding seizure
36 initiation and propagation. Here, we utilized well-established larval zebrafish seizure protocols and fast
37 confocal imaging of GCaMP-expressing fish to investigate the epileptic network properties at brain-wide
38 and single-cell levels. We revealed the rapid propagation of seizure activity from anterior-to-posterior
39 brain regions in zebrafish central nervous system. We also showed that micro-ensembles of neuronal
40 subpopulations are active during interictal-like periods in a manner similar to that seen in human
41 electrophysiology data sets. Our findings demonstrate that these non-invasive optical imaging
42 approaches will advance our understanding of the network basis underlying seizures and facilitate the
43 development of methods to suppress these events.

44 Introduction

45 Synchronization of neuronal networks is a commonly observed event in the brain and underlies
46 pathological generation and propagation of epileptic seizures. Although electrophysiological features of
47 an individual seizure event are well characterized using local field potential and/or single-unit
48 electrophysiological recordings (Grasse et al., 2013; Park et al., 2013; Schmidt et al., 2014; Truccolo et
49 al., 2014; Weiss et al., 2016), these approaches do not capture brain-wide spatiotemporal network
50 dynamics underlying these events. Efforts to image these networks have primarily been limited to small
51 microcircuits contained within brain slice preparations or imaging “windows” in head-restrained mice
52 (Trevelyan et al., 2006; Muldoon et al., 2013, 2015; Grosser et al., 2014; Kuzum et al., 2014; Hongo et
53 al., 2015; Lillis et al., 2015; Rossi et al., 2017; Wenzel et al., 2017; Liou et al., 2018). Recent advances in
54 imaging technology combined with stable expression of genetically encoded calcium indicators
55 (GCaMPs) (Tian et al., 2009; Akerboom et al., 2012; Chen et al., 2013) have led to a revolution in brain-
56 wide activity mapping. GCaMPs are employed in a range of model organisms; amongst these, larval
57 zebrafish (*Danio rerio*) offer an unparalleled combination of higher vertebrate relevance (including
58 human), optical transparency, and a small brain size (comprising approximately 100,000 neurons)
59 allowing spatial coverage of multiple brain regions. Moreover, the availability of transgenic zebrafish, in
60 which genetically-encoded GCaMPs are under the control of neuronal *elav13* or *NeuroD* promoters has
61 greatly facilitated the potential for assessing neural networks. Indeed, brain-wide imaging in GCaMP-
62 expressing zebrafish has already been used to monitor spatiotemporal patterns of neural activity during
63 fictive swimming (Ahrens et al., 2013a; Thiele et al., 2014), motor adaptation (Ahrens et al., 2012), visual
64 processing (Akerboom et al., 2012; Muto et al., 2013) and prey capture (Muto and Kawakami, 2013;
65 Semmelhack et al., 2014). During this time, zebrafish have also emerged as a valuable vertebrate model
66 for neurological disease, particularly for epilepsy (Hortopan et al., 2010; Ramirez et al., 2012; Stewart et
67 al., 2014; Grone and Baraban, 2015; Martín-Jiménez et al., 2015; Griffin et al., 2017). Combining these
68 advances, it is now possible to non-invasively monitor activity throughout the zebrafish nervous system
69 during an epileptic seizure event.

70 Brain-wide imaging during seizures, in contrast to invasive electrophysiological recordings, increases the
71 likelihood that network patterns will be discovered. To this end, we combined well-established acute
72 seizure (pentylentetrazole [PTZ]) (Baraban et al., 2005; Baxendale et al., 2012; Afrikanova et al., 2013;
73 Buenafe et al., 2013; Orellana-Paucar et al., 2013; Rahn et al., 2014; Siebel et al., 2015; Barbalho et al.,
74 2016; Copmans et al., 2018) and non-seizure hyperexcitability (4-Aminopyridine [4-AP]) models (Ellis et
75 al., 2012; Kumar et al., 2016; Cassar et al., 2017; Winter et al., 2017) with spinning disk confocal
76 microscopy, enabling fast (20 ~ 30 fps) *in vivo* imaging of network events. Imaging studies were
77 performed at brain-wide and single-cell resolution levels. As anesthetics can modify neuronal activity
78 (Greenberg et al., 2008), experiments were done using “awake” agarose-embedded larval zebrafish
79 paralyzed with pancuronium to reduce movement artifact. Simultaneous measurements of local field
80 potentials were used to confirm seizure activity. By analyzing brain-wide changes in calcium dynamics in
81 an acute seizure model, we revealed neuronal populations in telencephalon initiating ictal-like seizure
82 events that rapidly generalized to all central nervous system (CNS) regions. The spatiotemporal patterns
83 of calcium signal showed a rapid propagation of seizure activity from anterior-to-posterior brain regions.
84 Subsequent analysis of spontaneous activity patterns established a clear pattern of synchronization
85 during ictal-like seizure events consistent with a long-standing notion that seizures are a manifestation of
86 hypersynchronous neural networks. Automated calcium signal processing and spike detection confirmed
87 this high degree of synchronization at a single-neuron level. Finally, we showed that neuronal ensembles
88 (Tao et al., 2011; Truccolo et al., 2011, 2014; Miller et al., 2014) are active during interictal-like periods.
89 We suggest that these non-invasive optical imaging approaches could provide a more comprehensive
90 understanding of complex neuronal networks involved in the generation and propagation of seizures.

91

92 **Materials and Methods**

93 **Zebrafish lines**

94 All procedures followed National Institute of Health and the University of California, San Francisco
95 guidelines and were approved by the Institutional Animal Care and Use Committee. Calcium imaging
96 experiments were performed on the *Tg(neurod1:GCaMP6f)* line (Rupprecht et al., 2016) in the nacre

97 (*mitfa*^{-/-}) background (kindly provided by Dr. C. Wyart from Institut du Cerveau et de la Moelle épinière,
98 Paris) on 5-6 days post-fertilization (dpf). Adult zebrafish were maintained at 28° C on a 14:10 hour
99 light/dark cycle following standard methods. Larvae were raised in embryo media consisting of 0.03%
100 Instant Ocean (Aquarium Systems, Inc.) and 0.0002% methylene blue in reverse osmosis-distilled water.
101 At 5-6 dpf, zebrafish have not yet experienced sexual differentiation (Liew and Orbán, 2014).

102 **Calcium imaging and electrophysiology**

103 Zebrafish larvae were paralyzed in 300 μM pancuronium (Abcam), and then immobilized in a drop of 2%
104 low-melting point agarose in a recording chamber (Figure 1A). The recording chamber was placed on the
105 stage of a Zeiss Axiocam upright microscope using a 5x or 20x objective (for whole-brain and neuron-
106 level imaging respectively), Yokogawa CSU-X1 Spinning Disk Confocal and a 470 nm laser light source
107 (3i LaserStack). The recording chamber was filled with embryo media containing pancuronium (300 μM).
108 Epileptiform activities were induced by bath application of pentylenetetrazole (PTZ [10 mM], Sigma-
109 Aldrich) or 4-Aminopyridine (4-AP [4 mM], Sigma-Aldrich), and the fish were allowed to establish
110 consistent epileptiform activities for at least 40 min before imaging studies were initiated (Figure 1C).
111 Images of 512 x 512 pixels were acquired at 20 ~ 30 Hz with an EMCCD camera (Photometrics Evolve).
112 Multiple 5 min recordings (6000 ~ 9000 frames) were acquired for each experiment using SlideBook
113 software (3i Intelligent Imaging Innovations). To record local field potentials (LFP), a glass microelectrode
114 was placed under visual guidance in the optic tectum or cerebellum. Electrodes were filled with 2 M NaCl,
115 and electrical activity was recorded using an Axopatch 1D amplifier (Molecular Devices, Redwood City,
116 CA). Voltage records were low-pass filtered at 1 kHz (-3 dB, 8-pole Bessel), high-pass filtered at 0.1 Hz,
117 digitized at 10 kHz using a Digidata 1520 A/D interface, and stored on a PC computer running Axoclamp
118 software (Molecular Devices).

119 **Image analysis**

120 The raw images were first processed to correct motion drift using the Template Matching image
121 registration plugin for ImageJ. Regions of interest (ROIs) for brain regions and single neurons were
122 manually segmented with the ROI manager of ImageJ (Figure 1E, F). Corrected image stacks and ROI
123 segmentation file were then imported to MATLAB (MathWorks) for calcium fluorescence signal extraction

124 and analysis using the FluroroSNNAP software (Patel et al., 2015). The calcium fluorescence signal for
125 each brain region/neuron was obtained by averaging all pixels within the ROI. The fluorescence changes
126 ($\Delta F/F$) were calculated by subtracting each data point with the mean of the lower 50% of values within
127 previous 10 s sliding window and normalized to the mean of the lower 50% of values within previous 10 s
128 sliding window. Automated event detection was performed with the template-matching algorithm (Schultz
129 et al., 2009) included in the FluroroSNNAP. A time-varying correlation coefficient between fluorescence
130 trace and calcium transient templates (from the event waveform library) was calculated. Fluorescence
131 transients with amplitude $\Delta F/F > 0.1$ and correlation coefficient > 0.85 were identified as events. Local
132 maxima of the correlation coefficient trace identify the timestamps of calcium events. Since the algorithm
133 may sometimes give errors, the event train was then manually corrected by deleting falsely detected
134 events and adding events missed by the algorithm.

135 To determine the correlation between simultaneous calcium activity and LFP, the amplitude and duration
136 of ictal-like seizure events in PTZ-treated zebrafish were evaluated. The amplitude is the absolute value
137 of the maximum event peak, and the duration is the interval between the first and last points of the trace
138 leaving and returning the baseline.

139 **Network synchronization**

140 Whole-brain network synchronization was evaluated with the network analysis module of FluroroSNNAP.
141 Based on the instantaneous phase of the fluorescence trace of each brain region, a pair-wise phase
142 synchronization matrix was generated to identify patterns of network activity (Patel et al., 2015).
143 According to the matrix, an eigenvalue based algorithm was applied to calculate the global
144 synchronization index which range from 0 (non-coordinated activity) to 1 (completely synchronized
145 activity). For mathematical details see (Li et al., 2007). Briefly, the eigenvalues of the synchronization
146 matrix were calculated and then normalized to generate an array of synchronization indices. The largest
147 entry in this array is the global synchronization index. If the time series are fully uncorrelated, all elements
148 in the synchronization matrix would be 0, and the eigenvalue would be 0, resulting a global
149 synchronization index equal to 0. Alternatively, if the network was completely synchronized, all elements

150 in the synchronization matrix would be 1, and the maximal eigenvalue would be equal to the number of
151 time series with other eigenvalues falling to zero, resulting a global synchronization index equal to 1.

152 **Seizure propagation**

153 To determine the recruitment timing of each brain region to an ictal-like event, we took the time derivative
154 (slope) of the fluorescence trace (smoothed by taking moving average of 50 data points), and used the
155 local maxima (the fastest change in fluorescence) to identify the onset time point (Wenzel et al., 2017).
156 Each brain region has two data points corresponding to the left and right counterparts. We then
157 calculated the relative lag of each brain region with respect to the earliest onset within an ictal-like event
158 and normalized it to the interval between the earliest onset and the latest onset. Normalized relative lags
159 within an ictal-like event were divided into three quantile groups (first third - early, second third - middle
160 and third third - late), and the probability of each brain region falling into each quantile group was
161 calculated.

162 **Detection of ensemble events**

163 Ensemble events were defined as coactivation of a group of neurons in which a statistically significant
164 number of neurons are active compared with surrogate datasets. We used a sliding window to generate a
165 time series of coactivation of neurons by counting the number of events within a 0.5 s (10 frames)
166 window. The binary event data were shuffled 2000 times within neurons, and the sliding window counting
167 was performed. Frames with an observed number of coactive neurons > 99.9% of all surrogate values (p
168 < 0.001) were identified as highly active frames with ensemble event. To analyze the spatial extent of
169 neuronal ensembles, the distances between the ensemble centroid and individual neurons within the
170 ensemble were calculated using standard Euclidian distances.

171 **Experimental design and statistical analysis**

172 We used one-way ANOVA with Holm-Sidak post hoc analysis for multiple variable comparison, and Chi-
173 square test for onset timing distribution analysis, which were performed in Prism (GraphPad Software).
174 Correlation coefficients (R^2) between calcium and electrical signals were calculated in MATLAB
175 (MathWorks). Detection of neuronal ensembles was performed in MATLAB by comparing with surrogate
176 datasets (see Methods). Individual analyses are described in Results.

177

178 **Results**

179 To study synchronized neural networks, we used two well-characterized pharmacological models
180 employing bath application of PTZ (10 mM) or 4-AP (4 mM). These acute chemoconvulsant models work
181 through different mechanisms: (i) PTZ acts as a GABA_A receptor antagonist to disinhibit network activity
182 (Baraban et al., 2005; Baxendale et al., 2012; Afrikanova et al., 2013; Buenafe et al., 2013; Orellana-
183 Paucar et al., 2013; Rahn et al., 2014; Siebel et al., 2015; Barbalho et al., 2016; Copmans et al., 2018)
184 and (ii) 4-AP is a potassium channel blocker that enhances neuronal firing activity (Ellis et al., 2012;
185 Kumar et al., 2016; Cassar et al., 2017; Winter et al., 2017). Together, these acute models provide a
186 strategy to study recurrent spontaneous seizure events (PTZ) and non-seizure hyperexcitability (4-AP),
187 respectively.

188 **Multi-scale imaging of epileptiform activity**

189 High-speed confocal microscopy was used to monitor ictal-like activity in agar-embedded larval zebrafish
190 (Figure 1A) with neuronal expression of GCaMP (*neurod1:GCaMP6f*; Figure 1B). Larvae were
191 immobilized in agar and imaged using a 5x (brain-wide) or 20x (single-cell) objective. For brain-wide
192 studies, the confocal plane of view was adjusted to include forebrain (contains pallium and habenula),
193 optic tectum (contains neuropil and stratum periventriculare [SPV]), cerebellum and hindbrain (Figure 1D,
194 E). Regions of interest (ROI) were drawn manually over anatomical areas corresponding to major brain
195 regions, and fluorescence changes over time ($\Delta F/F$) were extracted from time-lapse movies acquired at
196 20 ~ 30 Hz (Figure 1E, F). In all PTZ-exposed larvae ($n = 43$), we observed large calcium transients at a
197 frequency of 1-2 events per min, which occurred synchronously across all brain ROIs consistent with a
198 generalized seizure classification (Figure 1E; Movie 3). Large calcium transients were not seen in Control
199 larvae bathed in embryo media ($n = 9$; Movie 1). As seizures are commonly associated with increased
200 synchrony in neuronal populations (Penfield and Jasper, 1954; Jiruska et al., 2013), we also monitored
201 calcium activity in SPV neurons within optic tectum microcircuits at single-cell resolution, which is
202 facilitated by the mosaic *neurod1*-driven expression of GCaMP6f in this brain region (Figure 1F).

203 Exposure to PTZ elicited waves of calcium activity that showed a high degree of synchrony across all
204 neurons (Movie 6).

205 To determine whether synchronous calcium events correspond to electrographic discharges, we
206 simultaneously monitored local field potentials (LFP) with an electrode placed in optic tectum SPV or
207 cerebellum (as noted in Figure 2B) in PTZ-treated larvae. Long-duration multi-spike ictal-like discharges
208 coincided with large-amplitude calcium transients in every recording (Figure 2A). The correlation between
209 whole-brain calcium transient amplitude and LFP amplitude was low (Figure 2C; $R^2 = 0.208$, $n = 54$
210 events from 10 PTZ-treated larvae). The relationship between whole-brain calcium transient duration and
211 electrographic event duration was approximately linear (Figure 2D; $R^2 = 0.839$, $n = 54$ events from 10
212 PTZ-treated larvae).

213 **Brain-wide network synchronization**

214 To investigate characteristics of synchronization, we analyzed brain-wide network dynamics in
215 hyperexcitable 4-AP-treated and epileptic PTZ-treated zebrafish. Age-matched untreated larvae were
216 studied as Controls. 4-AP and PTZ-treated larvae showed distinct activity patterns in both whole-brain
217 average fluorescence changes and LFP (Figure 3A). 4-AP treated larvae were characterized by high-
218 frequency short-duration spikes in LFP and frequent low-amplitude calcium transients. In contrast, PTZ-
219 treated larvae consistently exhibited recurrent high-amplitude long-duration ictal-like events in both LFP
220 and calcium traces, and significantly increased area under curve (AUC) in fluorescence changes
221 compared with Control and 4-AP-treated larvae (Figure 3B; $p < 0.001$, one-way ANOVA; $n = 4, 7$ and 7
222 fish for Control, 4-AP and PTZ condition, respectively).

223 Next, we analyzed the activity of subregions within the larval whole-brain network. Representative
224 fluorescence traces of each brain region (ROI numbering refers to Figure 1E) and corresponding
225 correlation matrices are shown in Figure 3C and D. Larvae exposed to 4-AP showed frequent short-
226 duration and low-amplitude calcium transients in cerebellum and hindbrain regions only. In contrast, PTZ-
227 treated larvae showed widespread high-amplitude and long-duration calcium transients across the entire
228 nervous system, and significantly increased brain-wide synchronization compared with Control and 4-AP-

229 treated larvae (Figure 3E; $p < 0.001$, one-way ANOVA; $n = 4, 7$ and 7 fish for Control, 4-AP and PTZ
230 condition, respectively). Whole-brain activity of Control, 4-AP and PTZ-treated fish are exemplified in
231 Movie 1, 2 and 3, respectively.

232 **Seizure propagation**

233 To determine brain regions recruited during seizure initiation and propagation, we analyzed calcium
234 changes in multiple brain regions (see Figure 1E) during PTZ exposure ($n = 30$ events from 7 PTZ-treated
235 larvae). Figure 4A shows representative fluorescence traces of each brain region during an ictal-like
236 event break-in. The red trace is the time derivative of $\Delta F/F$ moving average of 50 nearby data points, and
237 the local maxima position corresponds to the onset time point of the brain region. We calculated the
238 relative lag of each brain region and normalized it to the earliest-to-latest onsets interval. Arranging the
239 normalized relative lag of brain regions revealed a coarsely preserved temporal ordering across ictal-like
240 seizure events (Figure 4B). Figure 4C shows a color-coded onset time mapping from a representative
241 PTZ-induced ictal-like seizure events in one zebrafish (average of 4 ictal-like events). We then divided the
242 normalized relative lags within one ictal-like event into three quantile groups: early, middle and late
243 (Figure 4D), and calculated the probability of each brain region falling into each temporal group. This
244 analysis revealed a conserved propagation pattern from the anterior-to-posterior brain (Figure 4E; Chi-
245 square test $X^2(10) = 375.1$, $p < 0.001$; $n = 30$ events from 7 PTZ-treated larvae).

246

247 **Neuronal ensembles in optic tectum microcircuits**

248 Next, we investigated network dynamics of the optic tectum microcircuit at single-neuron resolution. We
249 analyzed individual SPV neuronal activity during interictal periods in representative Control, 4-AP and
250 PTZ-treated fish, since ictal-like seizure events involve over 90% of the neuronal population in the field of
251 view. Cerebellum activity, where baseline *neurod1:GCaMP6f* expression is prominent (see Figure 1B),
252 was also extracted as a reference of ictal-like events that generalize to the entire nervous system. Based
253 on binary event data generated from fluorescence changes with an automatic event detection algorithm
254 (Patel et al., 2015), we constructed raster plots of neuronal activity, and then used a sliding window

255 technique to generate a coactive neuron number time series (Figure 5A). Ensemble events, namely a
256 statistically significant number of coactive neurons compared with surrogate datasets, are marked by red
257 arrows (bottom panel in Figure 5A), and corresponding coactive neurons are colored red in the raster plot
258 (middle panel in Figure 5A). Chemoconvulsant (4-AP or PTZ) exposed larvae showed more frequent
259 ensemble event occurrence compared with Controls. The neural firing rate (i.e., number of events in a 5
260 min recording epoch) distribution shows that both drug exposures increase excitability within the optic
261 tectum network (Figure 5B). For Control fish, most neurons were inactive and firing at a low rate during
262 the recording epoch. For 4-AP-treated fish, about half of the neurons exhibit firing rates between 1 and
263 10 events per 5 min, with about 20% of neurons firing ≥ 10 events per 5 min. For PTZ-treated fish, no
264 neurons were silent and firing rates were between 1 and 8 events per 5 min. Neurons in PTZ-treated fish
265 showed significantly higher average firing rates than Control fish, and neurons in 4-AP-treated fish had
266 significantly higher average firing rate than both Control and PTZ-treated fish (Figure 5C; $p < 0.001$, one-
267 way ANOVA; $n = 75, 76$ and 68 neurons for Control, 4-AP and PTZ-treated fish, respectively).

268 We then analyzed the spatial properties of neuronal ensembles. Representative spatial distribution plots
269 of these ensembles (as noted in Figure 5A) onto the optic tectum are shown in Figure 5D. Ensembles
270 were detected in all Control, 4-AP and PTZ groups. Figure 5E shows the number of coactive neuron
271 distributions within these ensembles. Control fish data showed few frames with coactive neurons (6000
272 frames for each recording). While 4-AP-treated fish showed more frames with small coactive neuron
273 groups (number of coactive neurons < 5), consistent with overall network hyperexcitability. PTZ-treated
274 fish had more frames with larger coactive neuron groups (number of coactive neurons ≥ 5) than either
275 Control or 4-AP-treated fish. In an epileptic network that is able to generate ictal-like events (i.e., PTZ-
276 treated fish), spatially distributed ensembles are composed of larger groups of neurons.

277 The distance between ensemble centroid and each neuron within an ensemble also showed differences
278 between groups (Figure 5F, G). Ensembles observed in hyperexcitable 4-AP-treated fish network
279 showed significantly larger spatial extent than in Control or PTZ-treated fish ($p < 0.001$, one-way ANOVA;
280 $n = 17, 36$ and 42 ensemble neurons for Control, 4-AP and PTZ-treated fish, respectively). Network

281 dynamics of optic microcircuits are exemplified in Movie 4, 5 and 6 for Control, 4-AP and PTZ-treated fish,
282 respectively.

283

284 **Discussion**

285 Here we combined sensitive genetically encoded calcium indicators and high-speed multi-scale
286 monitoring of brain activity to characterize network dynamics in the CNS of larval zebrafish, following
287 chemoconvulsant treatment. Our experiments revealed that ictal-like seizures are characterized by
288 synchronous activation of the whole-brain network involving all major brain regions and propagate rapidly
289 in a preserved temporal ordering: from anterior-to-posterior brain. PTZ-induced seizure and 4-AP-induced
290 non-seizure hyperexcitability models showed distinct network dynamics in both whole-brain network and
291 optic tectum microcircuits. Analysis of individual neuronal activities during interictal periods revealed
292 neuronal ensembles in optic tectum, which demonstrated distinct properties in epileptic versus normal
293 brain.

294 Optical monitoring in larval zebrafish provides a unique opportunity to map neuronal activity in a brain-
295 wide manner. These measurements are not possible with electrophysiological approaches and led to
296 spatiotemporal analysis of seizure initiation and propagation across the zebrafish CNS. Previous imaging
297 studies using an acute PTZ seizure model in zebrafish focused on optical mapping of seizure propagation
298 (Tao et al., 2011) or brain activities coincident with tail movements (Turrini et al., 2017), using
299 mathematical modeling to reveal network connectivity changes during seizures (Rosch et al., 2018), and
300 functional profiling of drug action in multiple brain regions (Winter et al., 2017). Generalized brain-wide
301 activation during ictal-like seizure events was reported in these studies using acquisition speed ranges
302 from 1 Hz to 20 Hz. Here, using a fast spinning-disk confocal we observed similar patterns of brain activity
303 with acquisition speeds up to 30 Hz and discovered a reproducible anterior-to-posterior propagation
304 pattern of rapidly generalized optical seizures (Figure 4).

305 To confirm the correlation between electrographic and optical activity, we acquired LFP and calcium
306 imaging data simultaneously (Figure 2). A high degree of correlation was observed in event duration but

307 not in event amplitude (Figure 2C, D). This is not surprising, as LFP event amplitude is dependent on
308 electrode tip position in the brain relative to sources and sinks of current (Buzsáki et al., 2012), and
309 calcium signal amplitude is linked to focal plane and GCaMP expression intensity variabilities between
310 fish. Although both methods report generalized ictal-like seizure events consistently, LFP and calcium
311 imaging do not measure identical activity. For example, single and multi-unit background activity shown in
312 LFP recording in Control fish was not seen in corresponding calcium trace (Figure 3A, left); 4-AP fish
313 showed frequent high-amplitude spikes in LFP (Figure 3A, middle), but little to no fluorescence change
314 was observed in the recording region (optic tectum/cerebellum; ROI#7-10 in Figure 3C, middle). These
315 observations reveal the relative advantages and disadvantages of each approach. Compared with LFP
316 recording, GCaMP-based imaging provides superior spatial resolution but inferior detection sensitivity and
317 speed (Chen et al., 2013), which may not effectively detect sub-threshold synaptic transmission or
318 capture fast spikes seen in LFP recordings. Conversely, LFP recordings are limited to a single recording
319 site in the brain.

320 4-AP has been reported to induce ictal-like discharges *in vitro* (Galvan et al., 1982; Avoli et al., 2002) and
321 *in vivo* (Szente and Pongrácz, 1979; Peña and Tapia, 2000), but it is not a robust state in all conditions
322 (Perreault and Avoli, 1991, 1992; Mattia et al., 1993; Zhu et al., 2008; Avoli and Jefferys, 2016). In this
323 work, ictal-like seizure events were not consistently observed in 4-AP-exposed zebrafish larvae at a
324 concentration of 4 mM, except a fatal long-lasting burst after prolonged exposures (not shown), which is
325 consistent with other zebrafish-based imaging studies (Winter et al., 2017). 4-AP-induced neuronal
326 hyperexcitability revealed by LFP recordings (Figure 3) and imaging of microcircuit dynamics (Figure 5)
327 was also in line with previous reported behavioral manifestations in 4-AP-treated zebrafish (Kumar et al.,
328 2016) and provided us with an “interictal-like” state that was not complicated by the presence of ictal-like
329 activity.

330 When examining neuronal dynamics in optic tectum microcircuits, we detected ensembles of coactive
331 neurons during interictal periods and showed that, in PTZ-treated fish, ensembles were spatially
332 localized, while in 4-AP-treated fish, ensembles were smaller (contained less neurons) and dispersed
333 (Figure 5). Neuronal ensembles could also be detected in Control fish, but the ensemble event

334 occurrence was rare. Similar observations of functional clusters were reported in calcium imaging studies
335 from hippocampal slices prepared from chronically epileptic mice (Muldoon et al., 2013). Interestingly,
336 “microseizures”, which are discharges from highly confined neuron groups within ictal onset zones, have
337 been observed in intracranial recordings from microelectrode arrays in human patients with partial
338 epilepsy (Schevon et al., 2008, 2010; Stead et al., 2010). Although precise spatiotemporal information of
339 micro-discharge clusters is absent in these studies, it raises an intriguing hypothesis that ictal networks
340 are composed of sparse pathological microdomains that can generate microseizures, and the spreading
341 of microseizures results in ictal seizures (Stead et al., 2010). Here we employed a well-established acute
342 zebrafish seizure model and high-speed calcium imaging with single-cell resolution to map neural
343 activations. This strategy revealed neuronal ensembles in an ictal network (the optic tectum microcircuit),
344 which possibly correspond to human microseizure domains. Future studies using three-dimensional light
345 sheet imaging (Ahrens et al., 2013b; Portugues et al., 2014; Dunn et al., 2016) with enhanced scanning
346 speed could improve the neuron sampling and provide an even better understanding of the role of
347 neuronal ensembles in seizure generation and propagation.

348 In summary, we established a zebrafish-based calcium imaging platform to evaluate network dynamics
349 underlying recurrent seizures, including network synchronization, seizure propagation and neuronal
350 ensembles within local microcircuits. Future work with improved imaging techniques to explore the
351 interplay between micro-ensembles and macro-seizures, combined with zebrafish models mimicking
352 genetic forms of epilepsy, will provide insights into seizure prediction and suppression.

353

354 **References**

- 355 Afrikanova T, Serruys A-SK, Buenafe OEM, Clinckers R, Smolders I, Witte PAM de, Crawford AD,
356 Esguerra CV (2013) Validation of the Zebrafish Pentylentetrazol Seizure Model: Locomotor
357 versus Electrographic Responses to Antiepileptic Drugs. *PLOS ONE* 8:e54166.
- 358 Ahrens MB, Huang K-H, Narayan S, Mensh BD, Engert F (2013a) Two-photon calcium imaging during
359 fictive navigation in virtual environments. *Front Neural Circuits* 7 Available at:
360 <https://www.frontiersin.org/articles/10.3389/fncir.2013.00104/full> [Accessed October 17, 2018].
- 361 Ahrens MB, Li JM, Orger MB, Robson DN, Schier AF, Engert F, Portugues R (2012) Brain-wide neuronal
362 dynamics during motor adaptation in zebrafish. *Nature* 485:471–477.

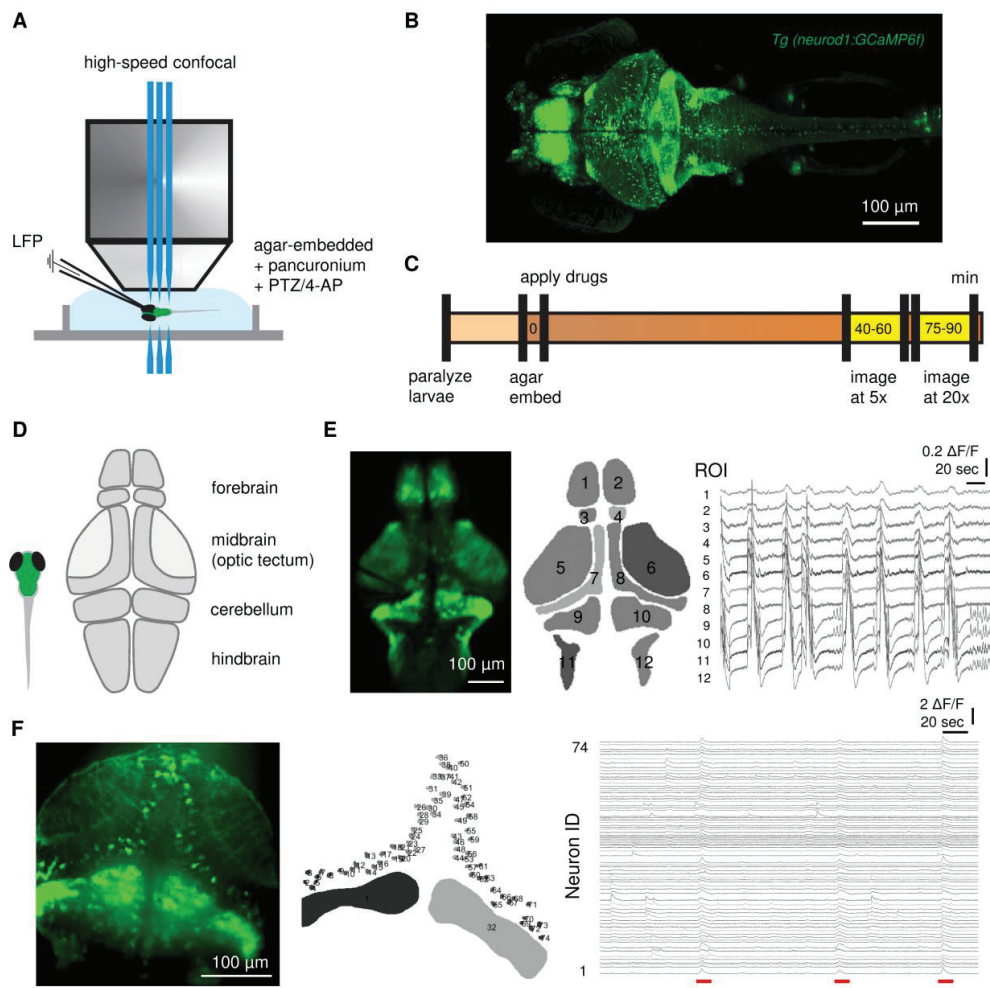
- 363 Ahrens MB, Orger MB, Robson DN, Li JM, Keller PJ (2013b) Whole-brain functional imaging at cellular
364 resolution using light-sheet microscopy. *Nat Methods* 10:413–420.
- 365 Akerboom J et al. (2012) Optimization of a GCaMP Calcium Indicator for Neural Activity Imaging. *J*
366 *Neurosci* 32:13819–13840.
- 367 Avoli M, D'Antuono M, Louvel J, Köhling R, Biagini G, Pumain R, D'Arcangelo G, Tancredi V (2002)
368 Network and pharmacological mechanisms leading to epileptiform synchronization in the limbic
369 system in vitro. *Prog Neurobiol* 68:167–207.
- 370 Avoli M, Jefferys JGR (2016) Models of drug-induced epileptiform synchronization in vitro. *J Neurosci*
371 *Methods* 260:26–32.
- 372 Baraban SC, Taylor MR, Castro PA, Baier H (2005) Pentylentetrazole induced changes in zebrafish
373 behavior, neural activity and c-fos expression. *Neuroscience* 131:759–768.
- 374 Barbalho PG, Lopes-Cendes I, Maurer-Morelli CV (2016) Indomethacin treatment prior to
375 pentylentetrazole-induced seizures downregulates the expression of il1b and cox2 and
376 decreases seizure-like behavior in zebrafish larvae. *BMC Neurosci* 17:12.
- 377 Baxendale S, Holdsworth CJ, Santoscoy PLM, Harrison MRM, Fox J, Parkin CA, Ingham PW, Cunliffe VT
378 (2012) Identification of compounds with anti-convulsant properties in a zebrafish model of
379 epileptic seizures. *Dis Model Mech:dmm*.010090.
- 380 Buenafe OE, Orellana-Paucar A, Maes J, Huang H, Ying X, De Borggraeve W, Crawford AD, Luyten W,
381 Esguerra CV, de Witte P (2013) Tanshinone IIA Exhibits Anticonvulsant Activity in Zebrafish and
382 Mouse Seizure Models. *ACS Chem Neurosci* 4:1479–1487.
- 383 Buzsáki G, Anastassiou CA, Koch C (2012) The origin of extracellular fields and currents—EEG, ECoG,
384 LFP and spikes. *Nat Rev Neurosci* 13:407–420.
- 385 Cassar S, Breidenbach L, Olson A, Huang X, Britton H, Woody C, Sancheti P, Stolarik D, Wicke K,
386 Hempel K, LeRoy B (2017) Measuring drug absorption improves interpretation of behavioral
387 responses in a larval zebrafish locomotor assay for predicting seizure liability. *J Pharmacol*
388 *Toxicol Methods* 88:56–63.
- 389 Chen T-W, Wardill TJ, Sun Y, Pulver SR, Renninger SL, Baohan A, Schreiter ER, Kerr RA, Orger MB,
390 Jayaraman V, Looger LL, Svoboda K, Kim DS (2013) Ultrasensitive fluorescent proteins for
391 imaging neuronal activity. *Nature* 499:295–300.
- 392 Copmans D, Orellana-Paucar AM, Steurs G, Zhang Y, Ny A, Foubert K, Exarchou V, Siekierska A, Kim Y,
393 De Borggraeve W, Dehaen W, Pieters L, de Witte PAM (2018) Methylated flavonoids as anti-
394 seizure agents: Naringenin 4',7-dimethyl ether attenuates epileptic seizures in zebrafish and
395 mouse models. *Neurochem Int* 112:124–133.
- 396 Dunn TW, Mu Y, Narayan S, Randlett O, Naumann EA, Yang C-T, Schier AF, Freeman J, Engert F,
397 Ahrens MB (2016) Brain-wide mapping of neural activity controlling zebrafish exploratory
398 locomotion *Calabrese RL*, ed. *eLife* 5:e12741.
- 399 Ellis LD, Seibert J, Soanes KH (2012) Distinct models of induced hyperactivity in zebrafish larvae. *Brain*
400 *Res* 1449:46–59.
- 401 Galvan M, Grafe P, Bruggencate GT (1982) Convulsant actions of 4-aminopyridine on the guinea-pig
402 olfactory cortex slice. *Brain Res* 241:75–86.

- 403 Grasse DW, Karunakaran S, Moxon KA (2013) Neuronal synchrony and the transition to spontaneous
404 seizures. *Exp Neurol* 248:72–84.
- 405 Greenberg DS, Houweling AR, Kerr JND (2008) Population imaging of ongoing neuronal activity in the
406 visual cortex of awake rats. *Nat Neurosci* 11:749–751.
- 407 Griffin A, Hamling KR, Knupp K, Hong S, Lee LP, Baraban SC (2017) Clemizole and modulators of
408 serotonin signalling suppress seizures in Dravet syndrome. *Brain* 140:669–683.
- 409 Grone BP, Baraban SC (2015) Animal models in epilepsy research: legacies and new directions. *Nat*
410 *Neurosci* 18:339–343.
- 411 Grosser S, Queenan BN, Lalchandani RR, Vicini S (2014) Hilar Somatostatin Interneurons Contribute to
412 Synchronized GABA Activity in an In Vitro Epilepsy Model. *PLOS ONE* 9:e86250.
- 413 Hongo Y, Takasu K, Ikegaya Y, Hasegawa M, Sakaguchi G, Ogawa K (2015) Heterogeneous effects of
414 antiepileptic drugs in an in vitro epilepsy model – a functional multineuron calcium imaging study.
415 *Eur J Neurosci* 42:1818–1829.
- 416 Hortopan GA, Dinday MT, Baraban SC (2010) Zebrafish as a model for studying genetic aspects of
417 epilepsy. *Dis Model Mech* 3:144–148.
- 418 Jiruska P, Curtis M de, Jefferys JGR, Schevon CA, Schiff SJ, Schindler K (2013) Synchronization and
419 desynchronization in epilepsy: controversies and hypotheses. *J Physiol* 591:787–797.
- 420 Kumar MG, Rowley S, Fulton R, Dinday MT, Baraban SC, Patel M (2016) Altered Glycolysis and
421 Mitochondrial Respiration in a Zebrafish Model of Dravet Syndrome. *eNeuro* 3:ENEURO.0008-
422 16.2016.
- 423 Kuzum D, Takano H, Shim E, Reed JC, Juul H, Richardson AG, de Vries J, Bink H, Dichter MA, Lucas
424 TH, Coulter DA, Cubukcu E, Litt B (2014) Transparent and flexible low noise graphene electrodes
425 for simultaneous electrophysiology and neuroimaging. *Nat Commun* 5:5259.
- 426 Li X, Cui D, Jiruska P, Fox JE, Yao X, Jefferys JGR (2007) Synchronization Measurement of Multiple
427 Neuronal Populations. *J Neurophysiol* 98:3341–3348.
- 428 Liew WC, Orbán L (2014) Zebrafish sex: a complicated affair. *Brief Funct Genomics* 13:172–187.
- 429 Lillis KP, Wang Z, Mail M, Zhao GQ, Berdichevsky Y, Bacskai B, Staley KJ (2015) Evolution of network
430 synchronization during early epileptogenesis parallels synaptic circuit alterations. *J Neurosci*
431 35:9920–9934.
- 432 Liou J, Ma H, Wenzel M, Zhao M, Baird-Daniel E, Smith EH, Daniel A, Emerson R, Yuste R, Schwartz
433 TH, Schevon CA (2018) Role of inhibitory control in modulating focal seizure spread. *Brain*
434 141:2083–2097.
- 435 Martín-Jiménez R, Campanella M, Russell C (2015) New Zebrafish Models of Neurodegeneration. *Curr*
436 *Neurol Neurosci Rep* 15:33.
- 437 Mattia D, Hwa GGC, Avoli M (1993) Epileptiform activity induced by 4-aminopyridine in guinea-pig and rat
438 neocortices. *Neurosci Lett* 154:157–160.
- 439 Miller JK, Ayzenshtat I, Carrillo-Reid L, Yuste R (2014) Visual stimuli recruit intrinsically generated cortical
440 ensembles. *Proc Natl Acad Sci* 111:E4053–E4061.

- 441 Muldoon SF, Soltesz I, Cossart R (2013) Spatially clustered neuronal assemblies comprise the
442 microstructure of synchrony in chronically epileptic networks. *Proc Natl Acad Sci* 110:3567–3572.
- 443 Muldoon SF, Villette V, Tressard T, Malvache A, Reichinnek S, Bartolomei F, Cossart R (2015)
444 GABAergic inhibition shapes interictal dynamics in awake epileptic mice. *Brain* 138:2875–2890.
- 445 Muto A, Kawakami K (2013) Prey capture in zebrafish larvae serves as a model to study cognitive
446 functions. *Front Neural Circuits* 7 Available at:
447 <https://www.frontiersin.org/articles/10.3389/fncir.2013.00110/full> [Accessed October 17, 2018].
- 448 Muto A, Ohkura M, Abe G, Nakai J, Kawakami K (2013) Real-Time Visualization of Neuronal Activity
449 during Perception. *Curr Biol* 23:307–311.
- 450 Orellana-Paucar AM, Afrikanova T, Thomas J, Aibuldinov YK, Dehaen W, Witte PAM de, Esguerra CV
451 (2013) Insights from Zebrafish and Mouse Models on the Activity and Safety of Ar-Turmerone as
452 a Potential Drug Candidate for the Treatment of Epilepsy. *PLOS ONE* 8:e81634.
- 453 Park YS, Hochberg LR, Eskandar EN, Cash SS, Truccolo W (2013) Early Detection of Human Epileptic
454 Seizures Based on Intracortical Local Field Potentials. *Int IEEEEMBS Conf Neural Eng Proc Int*
455 *IEEE EMBS Conf Neural Eng*:323–326.
- 456 Patel TP, Man K, Firestein BL, Meaney DF (2015) Automated quantification of neuronal networks and
457 single-cell calcium dynamics using calcium imaging. *J Neurosci Methods* 243:26–38.
- 458 Peña F, Tapia R (2000) Seizures and neurodegeneration induced by 4-aminopyridine in rat hippocampus
459 in vivo: role of glutamate- and GABA-mediated neurotransmission and of ion channels.
460 *Neuroscience* 101:547–561.
- 461 Penfield W, Jasper H (1954) *Epilepsy and the functional anatomy of the human brain*. Oxford, England:
462 Little, Brown & Co.
- 463 Perreault P, Avoli M (1991) Physiology and pharmacology of epileptiform activity induced by 4-
464 aminopyridine in rat hippocampal slices. *J Neurophysiol* 65:771–785.
- 465 Perreault P, Avoli M (1992) 4-aminopyridine-induced epileptiform activity and a GABA-mediated long-
466 lasting depolarization in the rat hippocampus. *J Neurosci Off J Soc Neurosci* 12:104–115.
- 467 Portugues R, Feierstein CE, Engert F, Orger MB (2014) Whole-brain activity maps reveal stereotyped,
468 distributed networks for visuomotor behavior. *Neuron* 81:1328–1343.
- 469 Rahn JJ, Bestman JE, Josey BJ, Inks ES, Stackley KD, Rogers CE, Chou CJ, Chan SSL (2014) Novel
470 Vitamin K analogs suppress seizures in zebrafish and mouse models of epilepsy. *Neuroscience*
471 259:142–154.
- 472 Ramirez IB-R, Pietka G, Jones DR, Divecha N, Alia A, Baraban SC, Hurlstone AFL, Lowe M (2012)
473 Impaired neural development in a zebrafish model for Lowe syndrome. *Hum Mol Genet* 21:1744–
474 1759.
- 475 Rosch RE, Hunter PR, Baldeweg T, Friston KJ, Meyer MP (2018) Calcium imaging and dynamic causal
476 modelling reveal brain-wide changes in effective connectivity and synaptic dynamics during
477 epileptic seizures. *PLOS Comput Biol* 14:e1006375.
- 478 Rossi LF, Wykes RC, Kullmann DM, Carandini M (2017) Focal cortical seizures start as standing waves
479 and propagate respecting homotopic connectivity. *Nat Commun* 8:217.

- 480 Rupperecht P, Prendergast A, Wyart C, Friedrich RW (2016) Remote z-scanning with a macroscopic voice
481 coil motor for fast 3D multiphoton laser scanning microscopy. *Biomed Opt Express* 7:1656–1671.
- 482 Schevon CA, Goodman RR, McKhann G, Emerson RG (2010) Propagation of Epileptiform Activity on a
483 Submillimeter Scale. *J Clin Neurophysiol Off Publ Am Electroencephalogr Soc* 27:406–411.
- 484 Schevon CA, Ng SK, Cappell J, Goodman RR, McKhann G, Waziri A, Branner A, Sosunov A, Schroeder
485 CE, Emerson RG (2008) Microphysiology of Epileptiform Activity in Human Neocortex. *J Clin*
486 *Neurophysiol Off Publ Am Electroencephalogr Soc* 25:321–330.
- 487 Schmidt H, Petkov G, Richardson MP, Terry JR (2014) Dynamics on Networks: The Role of Local
488 Dynamics and Global Networks on the Emergence of Hypersynchronous Neural Activity. *PLOS*
489 *Comput Biol* 10:e1003947.
- 490 Schultz SR, Kitamura K, Post-Uiterweer A, Krupic J, Häusser M (2009) Spatial Pattern Coding of Sensory
491 Information by Climbing Fiber-Evoked Calcium Signals in Networks of Neighboring Cerebellar
492 Purkinje Cells. *J Neurosci* 29:8005–8015.
- 493 Semmelhack JL, Donovan JC, Thiele TR, Kuehn E, Laurell E, Baier H (2014) A dedicated visual pathway
494 for prey detection in larval zebrafish Kiehn O, ed. *eLife* 3:e04878.
- 495 Siebel AM, Menezes FP, da Costa Schaefer I, Petersen BD, Bonan CD (2015) Rapamycin suppresses
496 PTZ-induced seizures at different developmental stages of zebrafish. *Pharmacol Biochem Behav*
497 139 Pt B:163–168.
- 498 Stead M, Bower M, Brinkmann BH, Lee K, Marsh WR, Meyer FB, Litt B, Van Gompel J, Worrell GA
499 (2010) Microseizures and the spatiotemporal scales of human partial epilepsy. *Brain* 133:2789–
500 2797.
- 501 Stewart AM, Braubach O, Spitsbergen J, Gerlai R, Kalueff AV (2014) Zebrafish models for translational
502 neuroscience research: from tank to bedside. *Trends Neurosci* 37:264–278.
- 503 Szente M, Pongrácz F (1979) Aminopyridine-induced seizure activity. *Electroencephalogr Clin*
504 *Neurophysiol* 46:605–608.
- 505 Tao L, Lauderdale JD, Sornborger AT (2011) Mapping Functional Connectivity between Neuronal
506 Ensembles with Larval Zebrafish Transgenic for a Ratiometric Calcium Indicator. *Front Neural*
507 *Circuits* 5 Available at: <https://www.frontiersin.org/articles/10.3389/fncir.2011.00002/full>
508 [Accessed December 3, 2018].
- 509 Thiele TR, Donovan JC, Baier H (2014) Descending Control of Swim Posture by a Midbrain Nucleus in
510 Zebrafish. *Neuron* 83:679–691.
- 511 Tian L, Hires SA, Mao T, Huber D, Chiappe ME, Chalasani SH, Petreanu L, Akerboom J, McKinney SA,
512 Schreier ER, Bargmann CI, Jayaraman V, Svoboda K, Looger LL (2009) Imaging neural activity
513 in worms, flies and mice with improved GCaMP calcium indicators. *Nat Methods* 6:875–881.
- 514 Trevelyan AJ, Sussillo D, Watson BO, Yuste R (2006) Modular Propagation of Epileptiform Activity:
515 Evidence for an Inhibitory Veto in Neocortex. *J Neurosci* 26:12447–12455.
- 516 Truccolo W, Ahmed OJ, Harrison MT, Eskandar EN, Cosgrove GR, Madsen JR, Blum AS, Potter NS,
517 Hochberg LR, Cash SS (2014) Neuronal Ensemble Synchrony during Human Focal Seizures. *J*
518 *Neurosci* 34:9927–9944.

- 519 Truccolo W, Donoghue JA, Hochberg LR, Eskandar EN, Madsen JR, Anderson WS, Brown EN, Halgren
520 E, Cash SS (2011) Single-neuron dynamics in human focal epilepsy. *Nat Neurosci* 14:635–641.
- 521 Turrini L, Fornetto C, Marchetto G, Müllenbroich MC, Tiso N, Vettori A, Resta F, Masi A, Mannaioni G,
522 Pavone FS, Vanzi F (2017) Optical mapping of neuronal activity during seizures in zebrafish. *Sci*
523 *Rep* 7:3025.
- 524 Weiss SA, Alvarado-Rojas C, Bragin A, Behnke E, Fields T, Fried I, Engel J, Staba R (2016) Ictal onset
525 patterns of local field potentials, high frequency oscillations, and unit activity in human mesial
526 temporal lobe epilepsy. *Epilepsia* 57:111–121.
- 527 Wenzel M, Hamm JP, Peterka DS, Yuste R (2017) Reliable and Elastic Propagation of Cortical Seizures
528 In Vivo. *Cell Rep* 19:2681–2693.
- 529 Winter MJ, Windell D, Metz J, Matthews P, Pinion J, Brown JT, Hetheridge MJ, Ball JS, Owen SF,
530 Redfern WS, Moger J, Randall AD, Tyler CR (2017) 4-dimensional functional profiling in the
531 convulsant-treated larval zebrafish brain. *Sci Rep* 7:6581.
- 532 Zhu L, Polley N, Mathews GC, Delpire E (2008) NKCC1 and KCC2 prevent hyperexcitability in the mouse
533 hippocampus. *Epilepsy Res* 79:201–212.
- 534



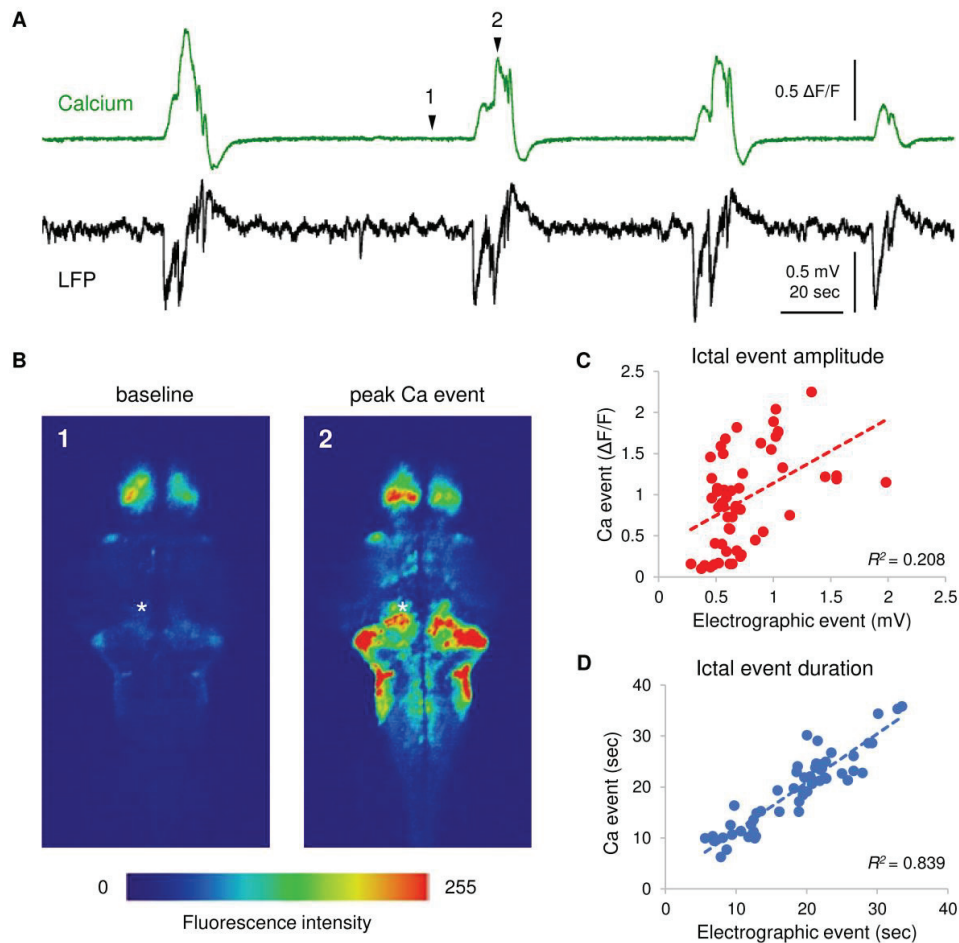
535

536 **Figure 1. High-speed confocal calcium imaging at different scales**

537 **A**, Experimental setup. Simultaneous local field potential (LFP) recording and fast confocal imaging (20 ~
538 30 fps) in agar-embedded larval zebrafish exposed to pancuronium (300 μ M) with PTZ (10 mM) or 4-AP
539 (4 mM). **B**, Representative high-resolution imaging of neurod1:GCaMP6f expressed larval zebrafish on 5-
540 6 days post fertilization (dpf). **C**, Experimental workflow. Recordings were obtained approximately 40 min
541 after drug application, and 5x and 20x objectives were used for whole-brain and neuron-level imaging
542 respectively. **D**, Schematic illustration depicting sub-regions of the larval zebrafish brain. **E**, Regions of
543 interest (ROI) and representative calcium traces ($\Delta F/F$) of PTZ-induced ictal-like events. 1,2: pallium; 3,4:

544 habenula; 5,6: neuropil; 7,8: stratum periventriculare (SPV); 9,10: cerebellum; 11,12: hindbrain. **F**,
545 Neuronal microcircuits within optic tectum and representative calcium traces of individual SPV neurons
546 with PTZ-induced ictal-like event break-ins (underlined in red). Cerebellum was included as an indicator
547 of ictal-like events that involve all brain regions. Scale bars as indicated in figure.

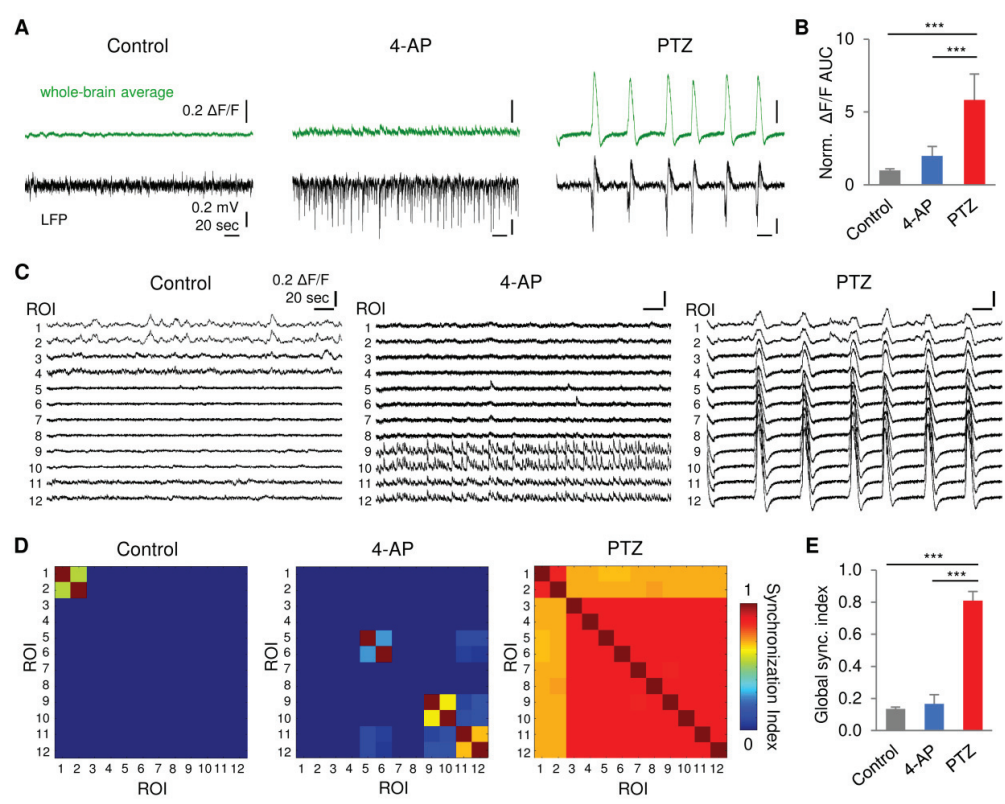
548



549

550 **Figure 2. Correlation between LFP and calcium transients**

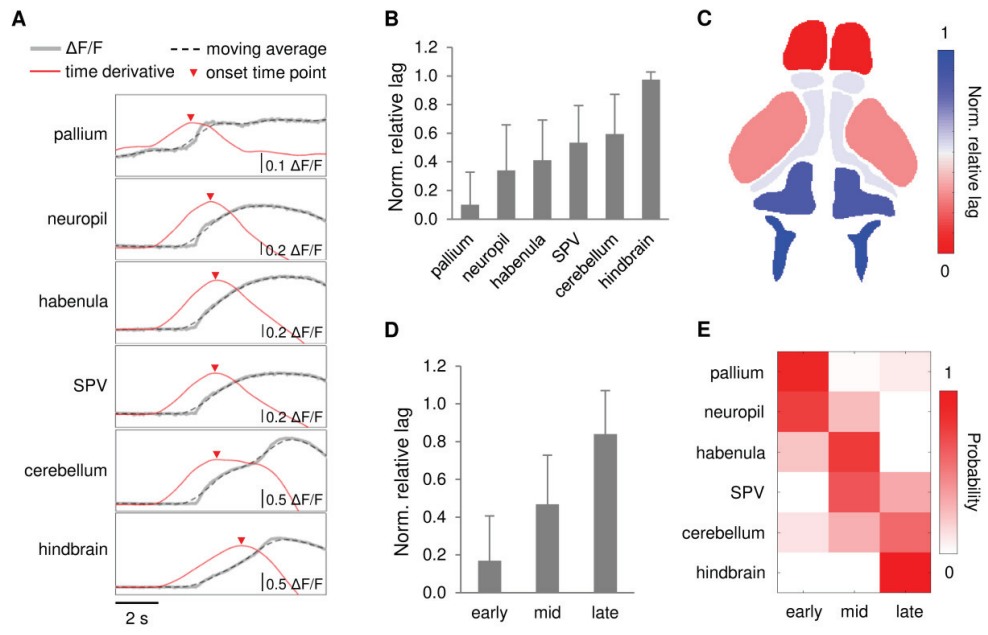
551 **A**, Representative simultaneous calcium traces (green) from the cerebellum and local field potential (LFP;
 552 black) recorded from optic tectum/cerebellum with recurrent PTZ-induced ictal-like seizures. Scale bars
 553 as indicated in figure. **B**, Fluorescence images of calcium activity during baseline and peak ictal-like
 554 event. The intensity of fluorescence is color coded as shown in the color bar. Event 1 and 2 as noted in **A**.
 555 Asterisk indicates the LFP recording site. **C**, **D**, Correlation between LFP and calcium transients in ictal-
 556 like event amplitude **C** and duration **D**. Corresponding correlation coefficient R^2 is indicated in figure. $n =$
 557 54 events from 10 PTZ-treated larvae.



558

559 **Figure 3. Brain-wide network synchronization**

560 **A**, Representative whole-brain average fluorescence changes ($\Delta F/F$; green) and LFP (black) recorded
 561 from Control, 4-AP and PTZ-treated larvae. **B**, Comparison of normalized area under curve of
 562 fluorescence changes (norm. $\Delta F/F$ AUC). **C**, Representative fluorescence changes of each brain region
 563 under different conditions. Regions of interest (ROI) refer to Figure 1E. **D**, Correlation matrices of whole-
 564 brain network activity for representative fish. **E**, Comparison of global synchronization (sync.) index. Scale
 565 bars as indicated in figure. $n = 4, 7$ and 7 fish for Control, 4-AP and PTZ condition, respectively. Error
 566 bars indicate standard deviation (SD). Statistical significance is indicated as *******, representing $p < 0.001$.

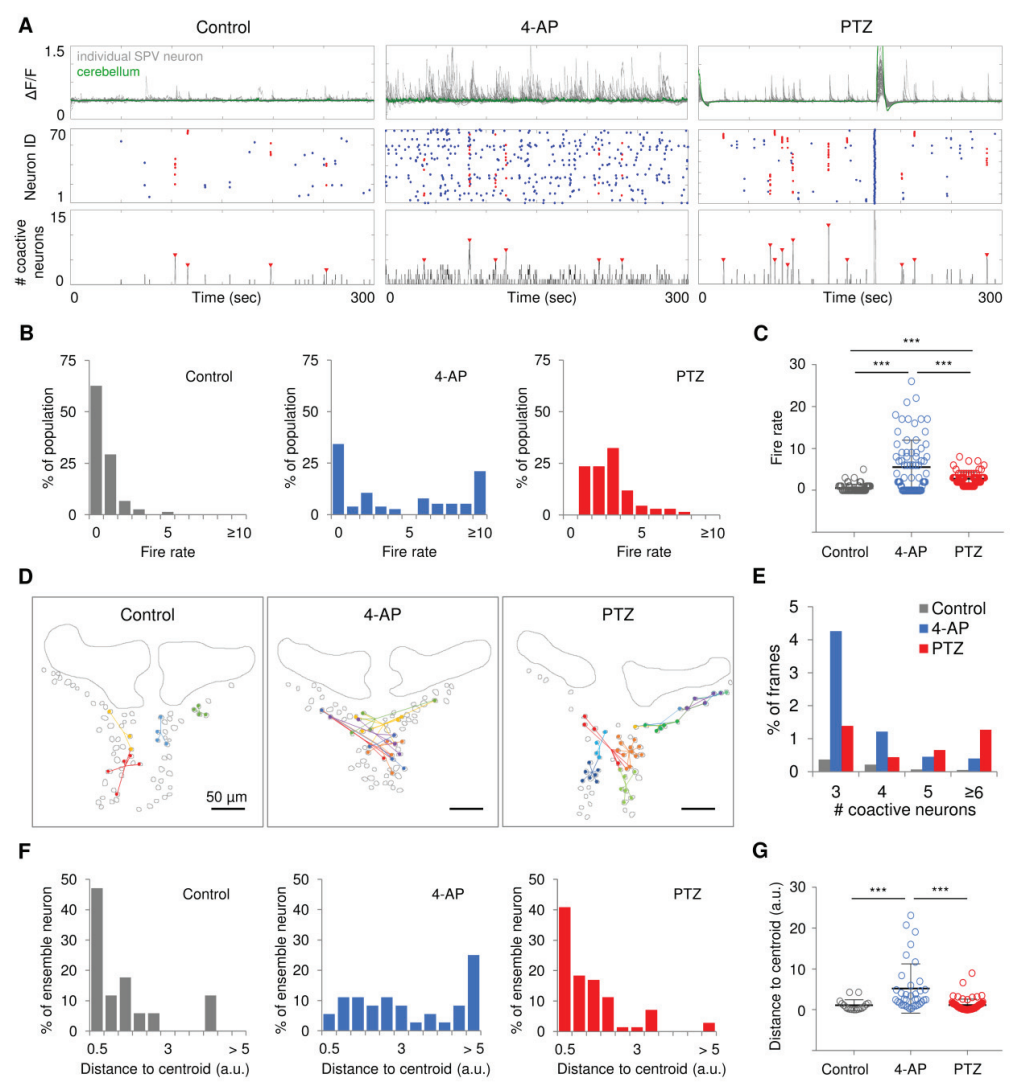


567

568 **Figure 4. Seizure propagation across the whole-brain**

569 **A**, Representative calcium trace for each brain region within an PTZ-induced ictal-like event. Event onset
 570 time points were determined by the local maxima of the time derivative of moving average (of 50 data
 571 points) of $\Delta F/F$. Scale bars as indicated in figure. **B**, Plot of normalized (norm.) relative lag from the
 572 earliest onset. **C**, Color-coded onset time mapping in a representative fish brain (average of 4 ictal
 573 events). **D**, Normalized relative lag for three quantile groups (first third early onset, second third middle
 574 onset, and third third late onset). **E**, Probability of brain regions falling into each quantile group. Chi-
 575 square test $\chi^2(10) = 375.1$, $p < 0.001$. Error bars indicate SD. $n = 30$ events from 7 PTZ-treated larvae.

576



577

578 **Figure 5. Neuronal ensembles in optic tectum microcircuits**

579 **A**, Representative calcium traces (grey, individual SPV neuron; green, cerebellum), neuron activation
 580 raster plot (red, ensemble neurons) and number of coactive neurons (ensembles were indicated by red
 581 arrow) of Control, 4-AP and PTZ-treated fish. Cerebellum activity was shown as an indicator of ictal-like
 582 events that involve all brain regions. **B**, **C**, Histogram **B** and distributions **C** of the neural firing rate (event
 583 count per 5 min). $n = 75, 76$ and 68 neurons for Control, 4-AP and PTZ-treated fish, respectively. **D**,

584 Spatial mapping of ensembles depicted in **A**. Dots in the same color represent coactive neurons, and
585 lines are distances from ensemble neurons to the corresponding ensemble centroid. Each ensemble is
586 indicated by a color. Scale bars as indicated in figure. **E**, Distribution of coactive neuron numbers as
587 percentage of frames (6000 frames for each recording). **F**, **G**, Histogram **F** and distributions **G** of
588 distances from ensemble neurons to the corresponding ensemble centroid. $n = 17, 36$ and 42 ensemble
589 neurons for Control, 4-AP and PTZ-treated fish, respectively. Error bars indicate SD. Statistical
590 significance is indicated as *******, representing $p < 0.001$.

591

592

593 **Movie 1, 2 and 3:** representative whole-brain imaging with 5x objective from Control, 4-AP and PTZ fish,
594 respectively. All movies played at 5x speed.

595 **Movie 4, 5, and 6:** representative imaging in optic tectum microcircuits with 20x objective from Control, 4-
596 AP and PTZ fish, respectively. All movies played at 5x speed.

597